Geophys. J. Int. (2000) **143,** 478–489

Matrix autoregressive analysis of free-oscillation coupling and splitting

Guy Masters, Gabi Laske and Freeman Gilbert

Institute of Geophysics and Planetary Physics, University of California, San Diego, La Jolla, CA 92093-0225, *USA. E-mail: glaske@ucsd.edu*

Accepted 2000 June 30. Received 2000 June 30; in original form 2000 January 20

SUMMARY

The study of the splitting and coupling of free oscillations can potentially provide some unique information about the Earth—in particular about how density varies laterally relative to shear velocity and bulk sound speed. Mode splitting has been studied for many years but it is clear that the time is ripe to revisit this field. In particular, the rapid expansion of the global seismic network and the occurrence of many large (and deep) earthquakes in the past few years means that mode-splitting analyses are capable of much higher precision than in the past. Some studies have already argued that 3-D density can be recovered (and that density variations are negatively correlated with shear velocity in the lower mantle). This result is controversial and we present some experiments that indicate that claims of density recovery with the current mode data set are premature. However, we believe that, with expanded data sets and new analysis techniques, the precision needed to recover the 3-D density structure of the Earth and its 3-D anelastic structure is now within our reach.

Key words: density, free oscillations, mode splitting.

INTRODUCTION

The Fiji event in March 1994 rekindled interest in observational low-frequency seismology (since it was the largest deep event to be digitally recorded since the 1970 Colombian event) but it was rapidly eclipsed by the Bolivian event in June 1994. Not only was the Bolivian event larger than the 1970 Colombian event but it was recorded by an unprecedented number of observatory-quality digital stations. The top two panels of Fig. 1 show details of a typical spectrum of a vertical-component recording of the event, illustrating the rich spectrum of high-Q overtones, which are sensitive to core structure. The anomalous splitting of multiplets such as ${}_{13}S_2$ is clearly visible. The event also excited other classes of modes that are sensitive to mantle structure and gave some very clear observations of low-order toroidal modes. Furthermore, on 1994 October 4, another great earthquake occurred in the southern Kuril Islands. This event was roughly the same size as the Bolivian event and was at about 50 km depth. It also strongly excited overtones. In fact, between 1994 and 1998, there were at least 21 extremely large earthquakes (Table 1) which have generated a significant new data set and caused a renaissance in observational low-frequency seismology.

Of course, in this age of 'high-resolution' tomography, one might wonder why research on observational aspects of the

Table 1. Earthquakes used in this study.

Event Name	Year.Day	Depth (km)	Moment (10^{20} Nm)	No. of records
Molucca Sea/Ceram Sea	1998.333	33	4.5	71
Balleny Islands Region	1998.084	33	18.2	81
Kamchatka	1997.339	33	5.3	110
Fiji Islands	1997.287	166	4.6	88
Santa Cruz Islands	1997.111	33	4.4	96
Peru	1996.317	33	4.6	97
Fiji Islands	1996.218	550	1.4	96
Flores	1996.169	587	7.3	90
Andreanof Island, Aleutians	1996.162	33	8.1	97
Irian Jaya	1996.048	33	24.1	103
Minahassa Peninsula, Celebes	1996.001	24	7.8	91
Kuril Islands	1995.337	33	8.2	83
Jalisco, Mexico	1995.282	33	11.5	96
Chile	1995.211	46	12.2	111
Loyalty Islands	1995.136	20	3.9	80
Honshu	1994.362	26	4.9	87
Kuril Islands	1994.277	54	30.0	101
Hokkaido	1994.202	471	1.1	76
Bolivia	1994.160	631	26.3	88
Java	1994.153	18	5.3	85
Fiji Islands	1994.068	562	3.1	83
South of Mariana Island	1993.220	59	5.2	72

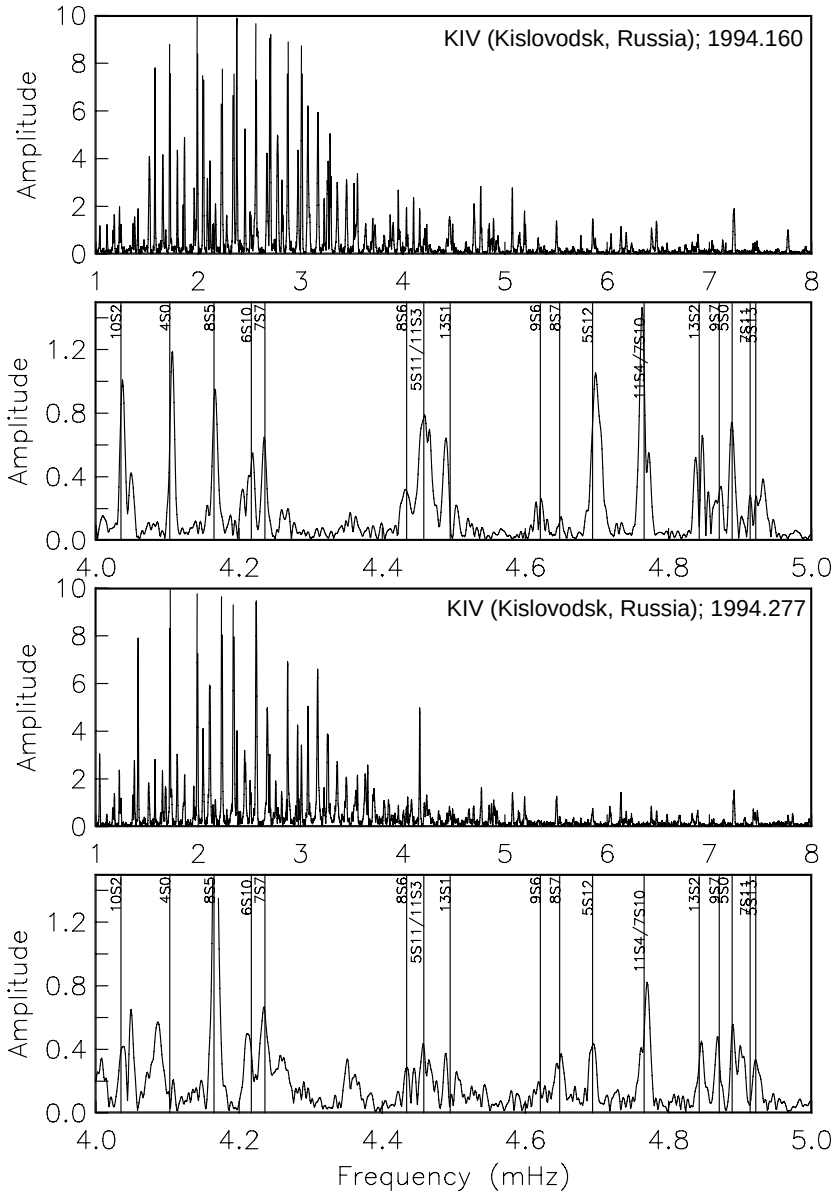

Figure 1. Top two panels show details of a typical spectrum from a vertical-component recording of the Bolivian (1994 June 9) event. 80 hr of data starting 10 hr after the event have been used to emphasize high-Q modes and a linear amplitude scale is used. Note the obvious splitting of some modes (e.g. ${}_{13}S_2$). The bottom two panels show details of a typical spectrum for the Kuril Islands (1994 October 4) event, which is also very overtone-rich.

Earth's free oscillations should continue to be of interest. Several points can be made.

(1) Free oscillation data are the only data capable of giving a direct picture of the 3-D density variation in the Earth (as well as being sensitive to V_s/V_p ratios). Such information is important for the physical interpretation of anomalies imaged by mantle tomography, and for deducing the driving forces for mantle flow.

(2) Although 3-D attenuation is difficult to determine with any data type, measurements of the complete splitting matrices of free oscillations are beginning to provide anelastic splitting functions suitable for input in inversions for 3-D Q structure.

(3) Free oscillations provide the 'big picture' since they filter out short-wavelength structure. Sometimes this can be a good thing (as in the determination of the relative rotation rate of the inner core—see below). Tomographic models that do not use free-oscillation data (or high-orbit surface wave data) frequently poorly represent the long-wavelength structure in the Earth (which also happens to be of the largest amplitude). In this respect, free-oscillation data are complementary to the body wave data sets commonly used in mantle tomography.

In this paper, we consider some of the problems in large-scale Earth structure that can be tackled using free-oscillation data.

STRUCTURE COEFFICIENTS AND SPLITTING FUNCTIONS

Since free oscillations 'see' the long-wavelength component of 3-D structure, it is convenient and efficient to parametrize 3-D structure ($\delta\mathbf{m} = \delta\rho,\ \delta\kappa,\ \delta\mu \ldots$) as an expansion in spherical harmonics:

$$\delta\mathbf{m}(r,\theta,\phi) = \sum \delta\mathbf{m}_s^t(r)\, Y_s^t(\theta,\phi)\,, \tag{1}$$

where Y_s^t is a fully normalized surface spherical harmonic. In general, $\delta\mathbf{m}$ may be complex and the imaginary part represents 3-D anelastic structure. A free-oscillation 'structure coefficient' is a depth-weighted average of the expansion coefficients of structure and will also generally have a real and imaginary part:

$$c_s^t + i d_s^t = \int \mathbf{M}_s(r) \cdot \delta\mathbf{m}_s^t(r)\, dr\,, \tag{2}$$

where $\mathbf{M}_s(r)$ is a vector of 'sensitivity kernels' that can be computed for any particular mode (Woodhouse & Dahlen 1978; Woodhouse 1980; Henson 1989; Dahlen & Tromp 1998). We refer to the c_s^t as the 'elastic structure coefficients' and the d_s^t as the 'anelastic structure coefficients'. Once structure coefficients have been measured, eq. (2) indicates that we have a linear inverse problem to solve for the coefficients in the spherical harmonic expansion of 3-D structure.

We often visualize the 3-D structure sensed by a mode by computing the elastic splitting function (e.g. Fig. 4):

$$f(\theta,\phi) = \sum_s \sum_{t=-s}^{s} c_s^t\, Y_s^t(\theta,\phi)\,. \tag{3}$$

A similar function can be generated for anelastic structure where the c_s^ts are replaced by d_s^ts. [Since the splitting functions are real, we have the relationship $c_s^{-t} = (-1)^t (c_s^t)^*$.]

The existing structure coefficients were mostly measured using the non-linear 'iterative spectral fitting' (ISF) technique (Ritzwoller *et al.* 1986, 1988; Giardini *et al.* 1987, 1988; Resovsky & Ritzwoller 1998; He & Tromp 1996). This technique requires a model of the source that may become quite inaccurate at moderate frequencies (10 mHz) for the extremely large earthquakes needed to excite overtones with a good signal-to-noise ratio (SNR). We have recently introduced a new method—the matrix AR method—that requires no information about the source (Masters *et al.* 2000a). A summary of the underlying theory is given below.

It is instructive to compare some of the different estimates of structure coefficients that have appeared in the literature. We find that there is often agreement for structure coefficients of degree 2 (e.g. Fig. 2) but agreement for structure coefficients of degrees 4 and 6 is typically poor and the errors are sufficiently large that the measurements are often indistinguishable from zero (e.g. Fig. 3). Sometimes, even the degree 2

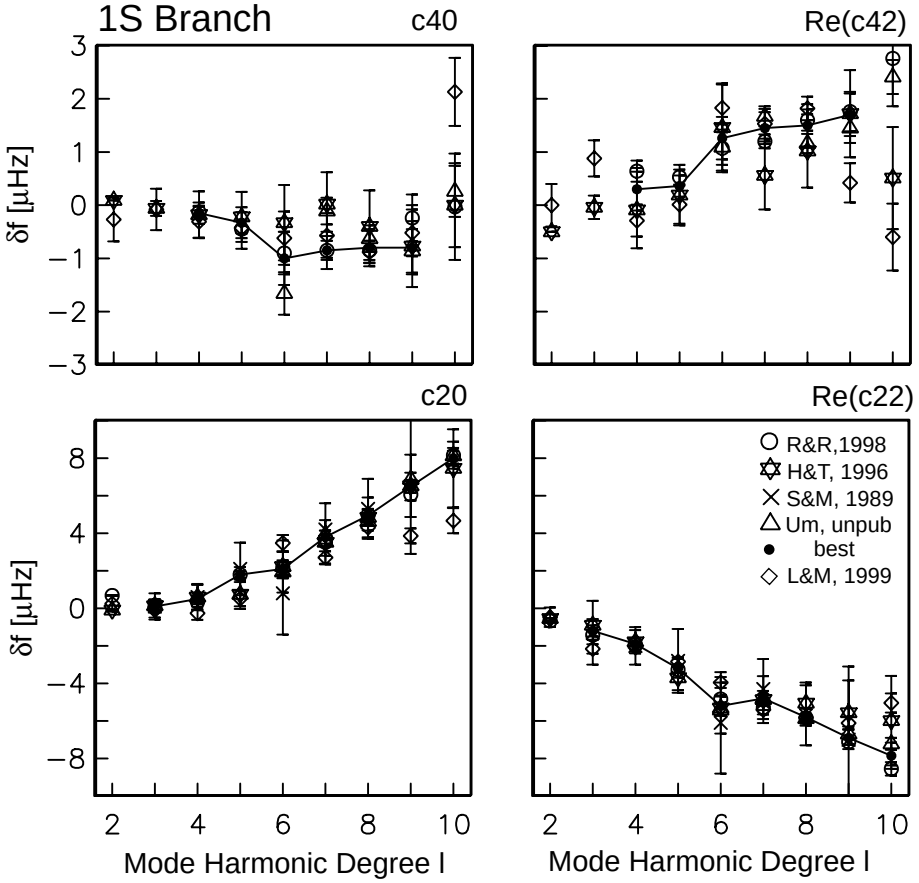

Figure 2. A selection of spheroidal-mode structure coefficients for the first overtone branch. Different symbols indicate the estimates of Resovsky & Ritzwoller (1998) (R&R), He & Tromp (1996) (H&T), Smith & Masters (1989) (S&M), unpublished values of Um (Um) and recent measurements of Laske & Masters (unpublished) (L&M) using the AR method. The black dots denote the 'best estimate', which is typically the median of all values. The $s = 2$ coefficients agree well between workers but the $s = 4$ coefficients show considerable scatter.

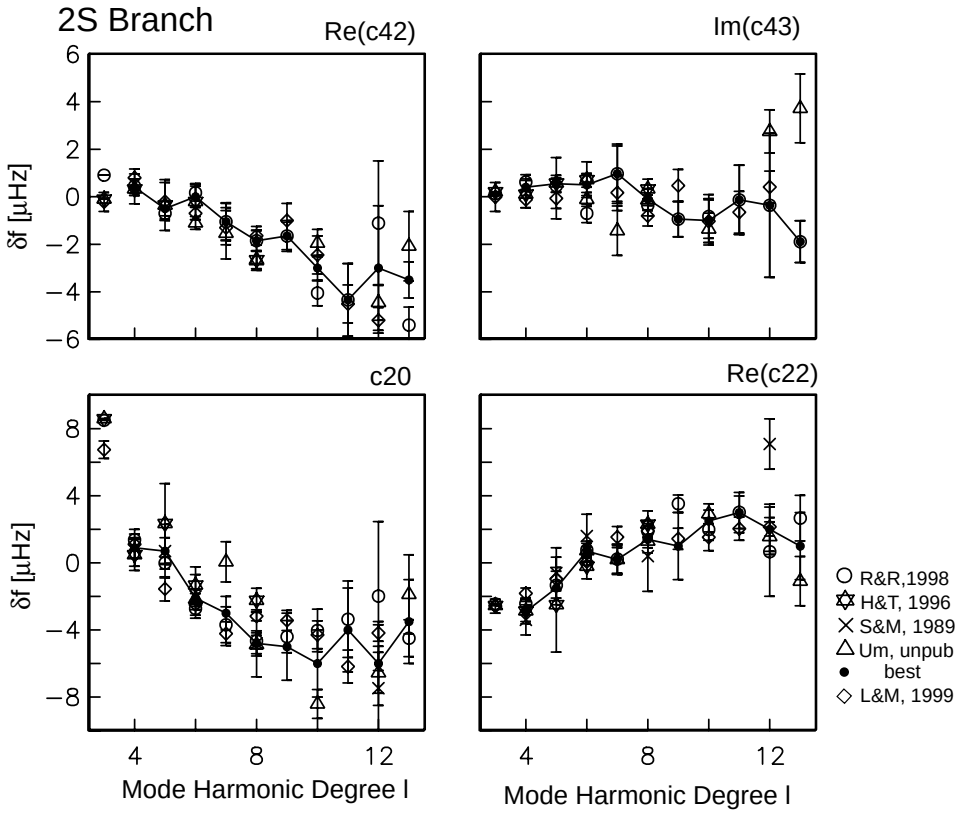

Figure 3. A selection of spheroidal-mode structure coefficients for the second overtone branch. In contrast to the ${}_1S_l$ branch, the c_s^ls for the ${}_2S_l$ modes are much more inconsistent between workers, even for $s=2$. For details see Fig. 2.

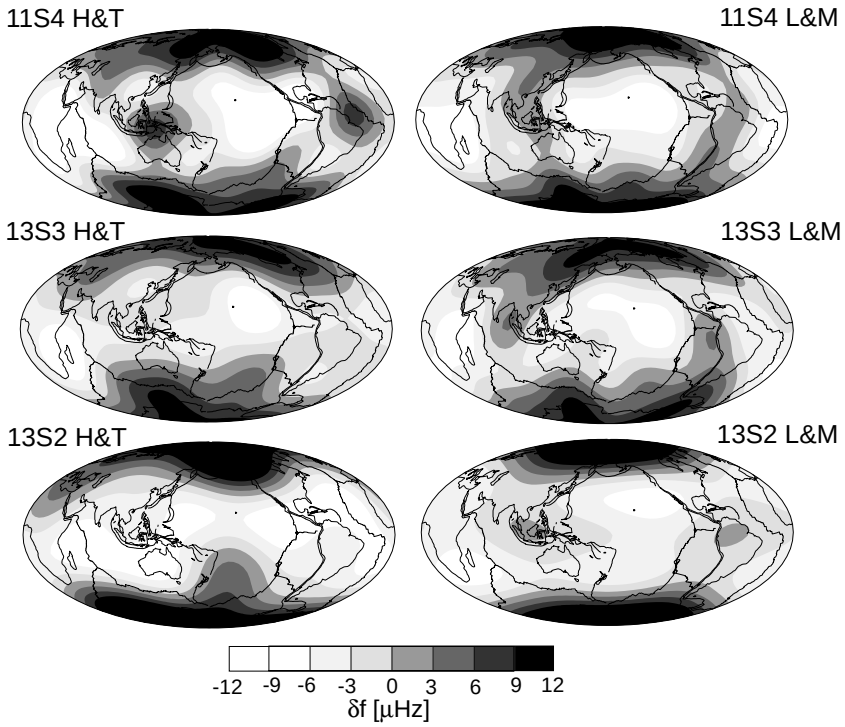

Figure 4. A comparison of splitting functions between He & Tromp (1996) and Laske & Masters (1999) for the three core-sensitive modes ${}_{11}S_4$, ${}_{13}S_3$ and ${}_{13}S_2$. The splitting functions are obtained using eq. (3) and the effects of rotation and ellipticity have been removed. There is considerable disagreement between these maps (the correlation of all maps is well below the 95 per cent confidence level for $s=4$, 6).

structure coefficients differ and the overall splitting functions of the modes correlate poorly (e.g. Fig. 4).

We have compiled a preliminary data set of structure coefficients of mantle-sensitive modes. This compilation is a mixture of our own work, the iterative spectral fitting results of Resovsky & Ritzwoller (1998) and He & Tromp (1996), and peak shift and surface wave dispersion data. Where possible, we use structure coefficients up to degree 6 but we note that most of the signal is in degree 2. The results of different studies are not always in agreement and we have used along-branch consistency arguments to choose 'best' values and assign credible errors (e.g. Figs 2 and 3). The data set includes ${}_0S_{3-60}$, ${}_1S_{3-10}$, ${}_2S_{4-13}$, ${}_3S_{6,8,9}$, ${}_5S_{4-8}$, ${}_0T_{4-50}$, ${}_1T_{1-9}$, and ${}_2T_{2,4,8}$.

PRELIMINARY INVERSION FOR 3-D DENSITY

The 'best-estimate' structure coefficient data set has been used (along with others) to perform joint inversions for bulk sound

Table 2. Fit of density models to modes.

Data set	χ^2/N initial	χ^2/N final	N
Experiment 1: $\delta\rho \propto \delta V_c$			
${}_nS_\ell$ ($s=2, 4, 6$)	29.4	0.7	1890
${}_nS_\ell$ ($s=2$)	93.5	1.4	375
${}_nT_\ell$ ($s=2, 4, 6$)	29.1	1.0	810
${}_nT_\ell$ ($s=2$)	38.5	1.0	215
Experiment 2: $\delta\rho \propto \delta V_s$			
${}_nS_\ell$ ($s=2, 4, 6$)	29.4	0.7	1890
${}_nS_\ell$ ($s=2$)	93.5	1.1	375
${}_nT_\ell$ ($s=2, 4, 6$)	29.1	1.0	810
${}_nT_\ell$ ($s=2$)	38.5	1.0	215
Experiment 3: $\delta\rho$ independent			
${}_nS_\ell$ ($s=2, 4, 6$)	29.4	0.6	1890
${}_nS_\ell$ ($s=2$)	93.5	0.9	375
${}_nT_\ell$ ($s=2, 4, 6$)	29.1	0.9	810
${}_nT_\ell$ ($s=2$)	38.5	0.8	215

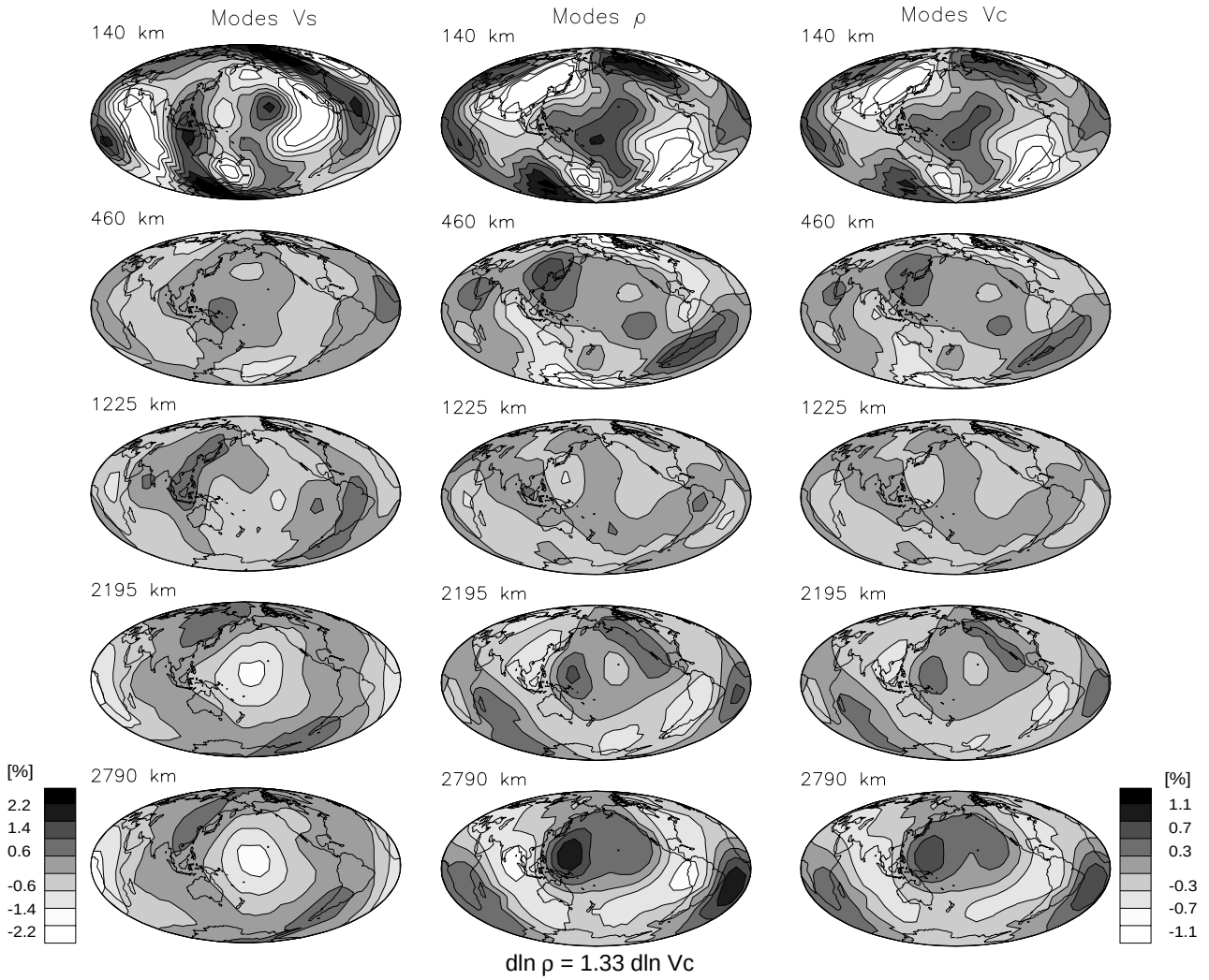

Figure 5. A joint inversion for shear velocity (V_s, left column) and bulk sound speed (V_c, right column) using the 'best estimate' structure coefficient data set described in the text and Figs 2 and 3. Each panel shows the relative variation of velocity at a particular depth inside the Earth. Density was scaled to be proportional to V_c and so is negatively correlated to V_s in the lower mantle. The scale of the density variations is the same as that of the variations in V_c, which is half the scale for V_s. Figs 5–7 may be viewed in colour in the on-line version of the journal (www.blackwell-synergy.com).

speed and shear velocity in the mantle (Masters *et al.* 2000b). Of course, the data are also sensitive to density and we normally accommodate this by scaling density perturbations to either shear velocity or bulk sound speed. Fig. 5 shows the model produced by inverting the mode data alone and scaling density to bulk sound speed (the scaling we use is equivalent to an Anderson–Grüneisen parameter, δ_S, of 2.5). Because bulk sound speed is negatively correlated with shear velocity in the lower mantle, this model implicitly has a density that is also negatively correlated with shear velocity—in agreement with the results of Ishii & Tromp (1999). For degree 2, where there is most signal, the model reduces χ^2/N from 93.5 to 1.4 for spheroidal modes and from 38.5 to 1.0 for toroidal modes (Table 2). The possibility that density is negatively correlated with shear velocity near the base of the mantle is currently of great interest since it might support a model of layered mantle convection recently proposed by Kellogg *et al.* (1999). This model has a chemically distinct layer above the core–mantle boundary (CMB) of highly variable thickness and is capable of explaining many geophysical and geochemical observations. Iron enrichment in this layer could lead to an anti-correlation of shear velocity and density.

To test whether the anti-correlation is robust, we repeat the inversion but now with density scaled to shear velocity (Fig. 6). The shear velocity model is almost identical to that shown in Fig. 5 and the bulk sound speed is now not as well correlated with the shear velocity in the upper mantle but is still strongly negatively correlated to the shear velocity model in the lower mantle. This model actually fits the data better than the one where density is forced to be proportional to bulk sound speed (χ^2/N is now 1.1 for spheroidal modes and 1.0 for toroidal modes) but the improvement in fit is marginal. A detailed study of the misfit shows that no mode branches are systematically misfitted for either model.

Finally, we performed an inversion where the density is allowed to go free. The result is shown in Fig. 7 and the fit is given in Table 2 (χ^2/N is now 0.9 for both spheroidal and toroidal modes). Interestingly, this model also shows a positive

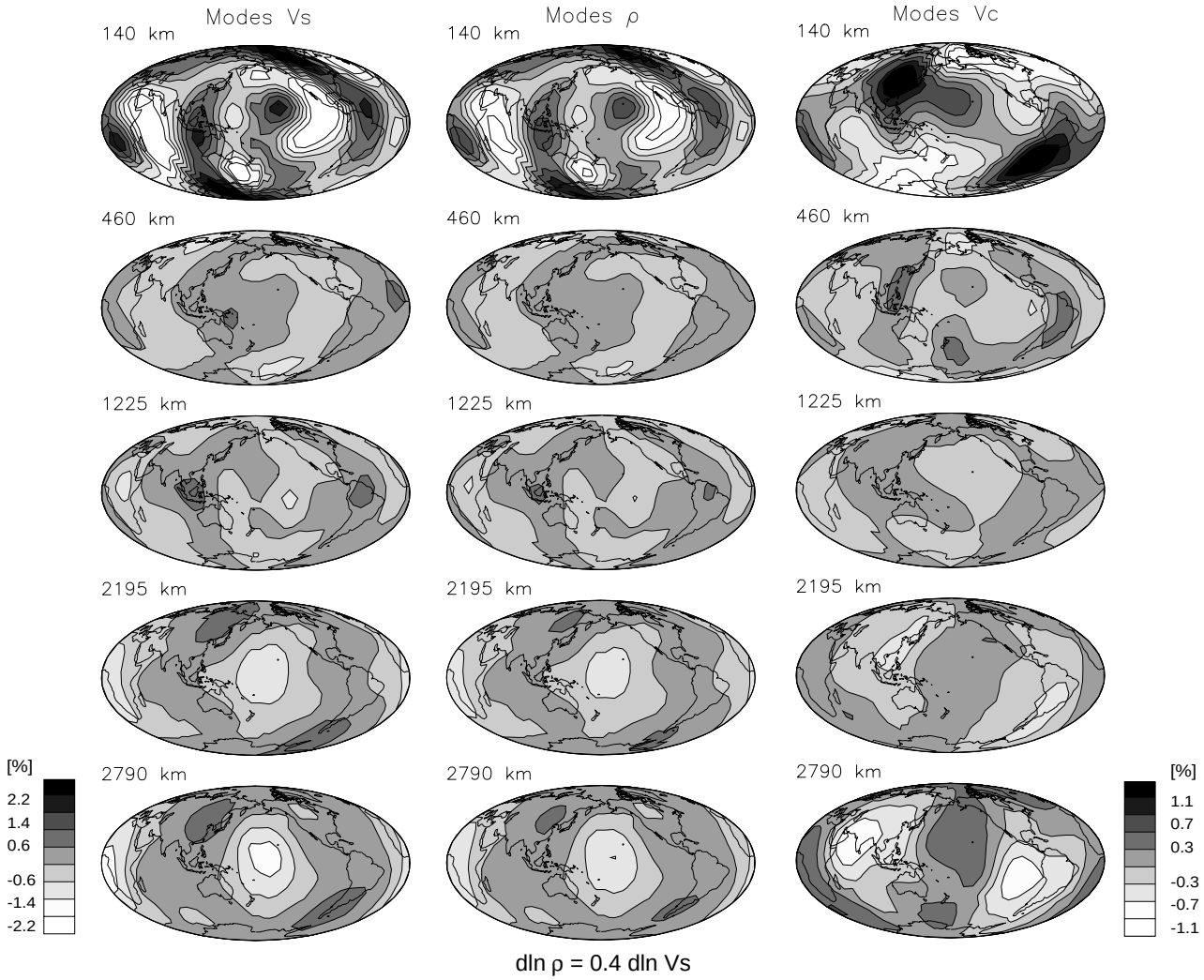

Figure 6. A joint inversion for shear velocity (V_s, left column) and bulk sound speed (V_c, right column) but now with the density scaled to be proportional to V_s. Note that in both inversions, V_s and V_c are anti-correlated at the base of the mantle. This is a stable feature that is seen in many joint V_c/V_s models (Masters *et al.* 2000b). The scale of the density variations is the same as that of the variations in V_c, which is half the scale for V_s.

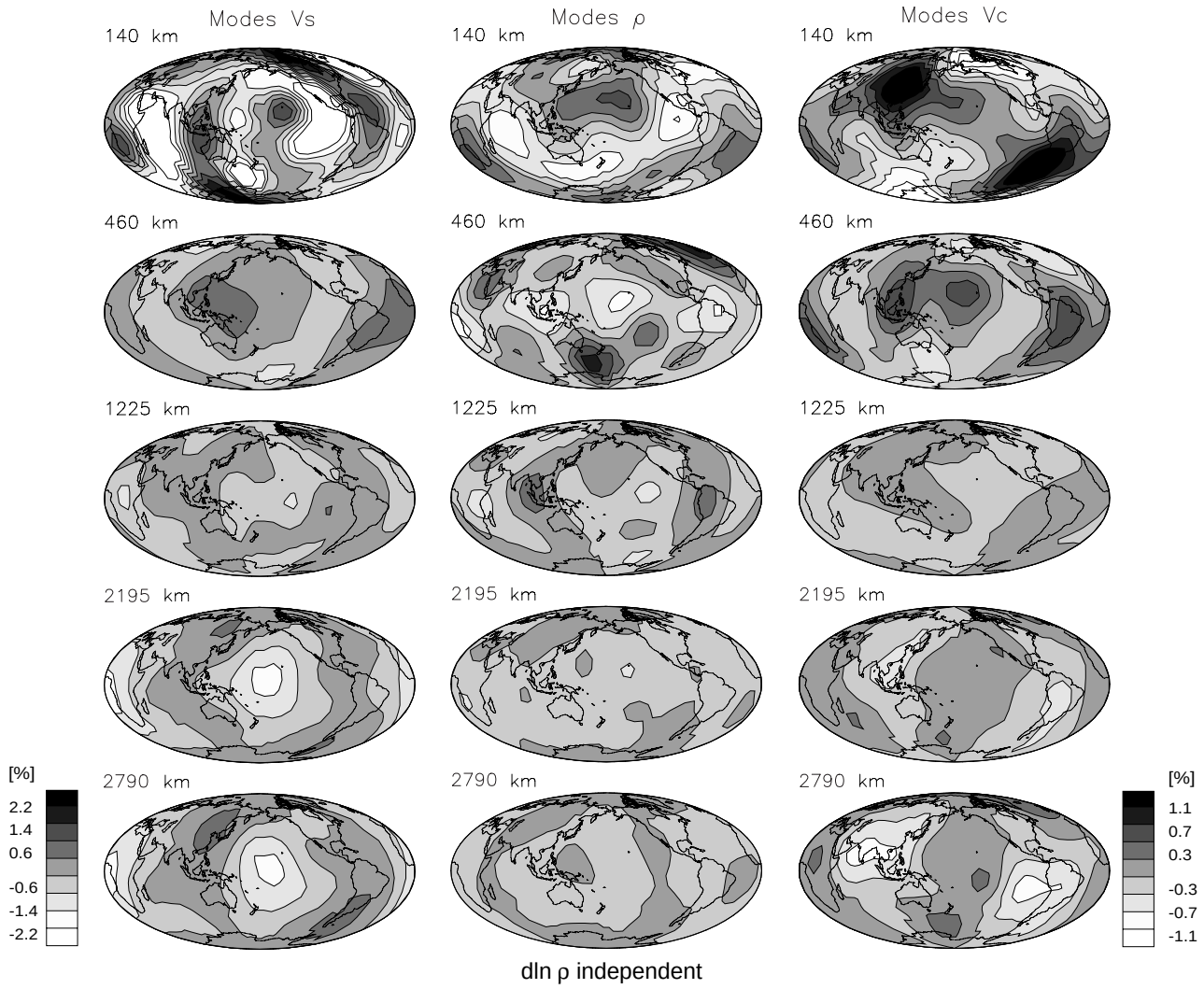

Figure 7. A joint inversion for shear velocity (V_s, left column) and bulk sound speed (V_c, right column) but now with the density being solved for independently. In this inversion, as in the two previous ones, V_s and V_c are anti-correlated at the base of the mantle. Also note that density and shear velocity are not anti-correlated at the base of the mantle, which is in contrast to what was found in the recent study of Ishii & Tromp (1999). The scale of the density variations is the same as that of the variations in V_c, which is half the scale for V_s.

correlation of density to shear velocity in the lowermost model, again in contradiction to the results of Ishii & Tromp (1999), although the difference in fit to the data for any of the models is rather small.

We take these results to imply that the current data set cannot distinguish between models in which density is positively or negatively correlated to shear velocity in the lower mantle. It is interesting to note, however, that the anti-correlation of bulk sound speed to shear velocity near the base of the mantle does not depend on the choice of scaling for density. The anti-correlation persists when body wave and surface wave data sets are included in the inversion and is a robust feature that is also seen by other workers (e.g. Su & Dziewonski 1997). Both the anti-correlation of V_s and V_c and the high values for the ratio of shear versus compressional velocity variations $R = d \ln v_s / d \ln v_p$ with values that exceed 2.0 are indicative that the 3-D structure at the base of the mantle cannot be caused by purely subsolidus thermal effects but that compositional changes and/or partial melt play a significant role (see Masters *et al.* 2000b for details).

In following sections, we show how more precise measurements can be obtained. A potential future application to the determination of 1-D density by Coriolis coupling and splitting parameters is given in Appendix A.

THE MATRIX AR TECHNIQUE

For simplicity, we consider the theory for an isolated multiplet—the extension to overlapping and/or coupled multiplets is trivial. Our starting point is the representation of an isolated split multiplet first given by Woodhouse & Girnius (1982) (see also Landau & Lifshitz 1958, Section 40):

$$u_j(t) = \sum_{k=1}^{2\ell+1} R_{jk} a_k(t)\, \mathrm{e}^{i\bar{\omega}t} \qquad \text{or} \qquad \mathbf{u}(t) = \mathbf{R} \cdot \mathbf{a}(t)\, \mathrm{e}^{i\bar{\omega}t}, \tag{4}$$

where the real part is understood. The jth row of R_{jk} is a $2\ell+1$ vector of spherical harmonics that describe the motion of

the spherical-earth singlets at the jth receiver and is readily calculated. $\bar{\omega}$ is the multiplet degenerate frequency and $\mathbf{a}(t)$ is a slowly varying function of time, where the autoregressive (or AR) property is given by

$$\mathbf{a}(t) = \exp(i\mathbf{H}t) \cdot \mathbf{a}(0), \tag{5}$$

where $\mathbf{a}(0)$ is a $2\ell+1$ vector of spherical-earth singlet excitation coefficients that can be computed if the source mechanism of the event is known. $\mathbf{H}$ is the complex *splitting matrix* that completely characterizes the effect of 3-D elastic and anelastic structure on the mode, so $\mathbf{H}$ is what we want to solve for.

For each event we form the 'receiver strips' (e.g. Fig. 8)

$$\mathbf{b}(t) = \mathbf{R}^{-1} \cdot \mathbf{u}(t) = \exp[i(\mathbf{H} + \mathbf{I}\bar{\omega})t] \cdot \mathbf{a}(0). \tag{6}$$

This operation is stable since $\mathbf{R}$ is well conditioned for a typical distribution of stations. Note that $\mathbf{b}(t)$ satisfies a recurrence in time given by

$$\mathbf{b}(t+\delta t) = \mathbf{P}(\delta t) \cdot \mathbf{b}(t), \tag{7}$$

where

$$\mathbf{P}(\delta t) = \exp[i(\mathbf{H} + \mathbf{I}\bar{\omega})\delta t]. \tag{8}$$

The set of equations (7) and (8) gives the theoretical basis for estimating the splitting matrix and does not depend on the source. If we can recover $\mathbf{P}$ from the data, it is straightforward to obtain $\mathbf{H}$ using an eigenvalue decomposition of $\mathbf{P}$. To recover $\mathbf{P}$, we calculate the spectra of the data, $\mathbf{u}(t)$, at different time lags, δt, and then form the receiver strips using eq. (8). We write the spectra of the receiver strips formed from data lagged by $n\delta t$ as $\mathbf{b}_n(\omega)$. Transposing eq. (9) gives a matrix system where each row is a $2\ell+1$ vector of receiver strips at a particular frequency:

$$\begin{bmatrix} \mathbf{b}_{n+1}^{\mathrm{T}}(\omega_1) \\ \mathbf{b}_{n+1}^{\mathrm{T}}(\omega_2) \\ \mathbf{b}_{n+1}^{\mathrm{T}}(\omega_3) \\ \vdots \end{bmatrix} = \begin{bmatrix} \mathbf{b}_{n}^{\mathrm{T}}(\omega_1) \\ \mathbf{b}_{n}^{\mathrm{T}}(\omega_2) \\ \mathbf{b}_{n}^{\mathrm{T}}(\omega_3) \\ \vdots \end{bmatrix} \cdot \mathbf{P}^{\mathrm{T}} \tag{9}$$

or

$$\mathbf{B}_{n+1} = \mathbf{B}_n \cdot \mathbf{P}^{\mathrm{T}}. \tag{10}$$

Eq. (10) can be made overdetermined and solved for $\mathbf{P}^{\mathrm{T}}$ by stacking receiver strips from different events and, in principle, the SNR can be improved by taking multiple lags and by using multiple tapers. Note that stacking events is particularly straightforward since the procedure does not require the source mechanism to be known. In fact, our technique is insensitive to both the temporal and the spatial locations of the event and is valid for overlapping events, provided the lagged windows include no new sources.

The splitting matrix and the structure coefficients are linearly related. To separate elastic and anelastic effects, we perform the unique decomposition

$$\mathbf{H} = \mathbf{E} + i\mathbf{A}, \tag{11}$$

with $\mathbf{E} = (\mathbf{H} + \mathbf{H}^{\mathrm{H}})/2$ and $i\mathbf{A} = (\mathbf{H} - \mathbf{H}^{\mathrm{H}})/2$, where superscript H indicates Hermitian transpose. Both $\mathbf{E}$ and $\mathbf{A}$ are Hermitian and can be written

$$E_{mm'} = \sum_s \gamma_s^{mm'} c_s^{m-m'}; \qquad A_{mm'} = \sum_s \gamma_s^{mm'} d_s^{m-m'}, \tag{12}$$

where we have removed the effects of centrifugal force and ellipticity, the γs are integrals over three spherical harmonics that are easy to compute, and the c_s^t and d_s^t are the structure coefficients of eq. (2).

From eqs (2) and (12) we see that $\mathbf{E}$ and $\mathbf{A}$ can be inverted directly for 3-D structure. Alternatively, eq. (12) can be solved for the structure coefficients and then eq. (2) for 3-D structure. The relation (12) can easily be solved for the c_s^ts using the orthogonal transformation (Gilbert & Woodhouse 2000)

$$\sum_{m'} \gamma_s^{m'+t,m'} \gamma_{s'}^{m'+t,m'} = \text{const}\ \delta_{ss'}.$$

Penalties may be included for rough structure (i.e. high s).

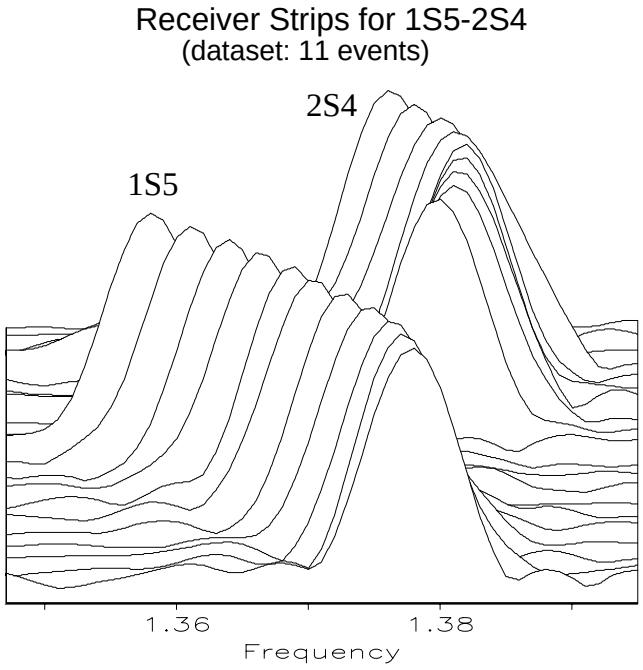

Figure 8. A stack of receiver strips for the weakly coupled mode pair ${}_1S_5/{}_2S_4$. Strips were stacked for the 11 largest events since 1994 (see Table 1) to enhance the SNR. Each strip is a linear amplitude spectrum normalized to unit peak amplitude. The panels show a joint determination of the strips for both modes with the nine strips of ${}_2S_4$ at the back. A record length of 70 hr was used, which is close to the optimal record length for the faster decaying mode ${}_1S_5$.

AN EXAMPLE: COUPLED MODES

Measuring the complete splitting matrix of coupled modes gives us the opportunity to constrain structure of odd harmonic

degree. An example for the weakly coupled pair of multiplets ${}_2S_4$ and ${}_1S_5$ is summarized Figs 8 and 9. The receiver strips visually separate the two coupled multiplets (Fig. 8). Measured and predicted splitting matrices are shown in Fig. 9. The theoretical splitting matrices were obtained using the coupled-mode code of Park & Gilbert (1986). Rotation of the Earth, ellipticity and elastic whole-mantle model S16B30 (Masters *et al.* 1996), but no 3-D attenuation, were included in the calculations. While the diagonal self-coupling blocks of **H** constrain structure of even degree (up to $s=8$ for ${}_2S_4$ and $s=10$ for ${}_1S_5$), the off-diagonal cross-coupling blocks of **H** contain information on odd-degree structure $1\leq s\leq 9$. While our data set is now large enough to constrain reliably the elastic splitting matrices **E** for a variety of isolated modes (see Masters *et al.* 2000a), the number of available events is still too small to determine odd-order structure with the same precision. However, the good agreement of the basic signal in the cross-coupling blocks with that of predictions from a mantle model indicates that this will no longer be true in the not too distant future.

We also have to be aware that analysing a strongly coupled mode as if it were an isolated mode may lead to biased results. The strong coupling effects for mode pair ${}_2S_0$–${}_7S_2$ is summarized in Figs 10 and 11. The receiver strips are no longer visually isolated and the spectral lines do not represent individual singlets. The lower panel of Fig. 10 indicates that ${}_2S_0$ interacts with the $m=0$ line of ${}_7S_2$ most strongly and the coupling causes the lines to repel each other. In our example, the coupling (using only a mantle model) causes a frequency shift for ${}_2S_0$ of 0.33 μHz, which is about twice the value of a conservatively chosen measurement error for ${}_2S_0$. Hence, measuring the frequency of ${}_2S_0$ ignoring the strong coupling to ${}_7S_2$ gives values that are too low (see also Park 1990). Also note that the measured receiver strips are more complicated than the predicted ones. This is caused by the large-amplitude 3-D structure in the inner core, which was ignored in the synthetic example. Also note that the frequencies of ${}_7S_2$ are spread over a much larger range than predicted. This phenomenon is know as 'anomalous splitting' and is also attributed to the strong anisotropy in the inner core (e.g. Woodhouse *et al.* 1986). Predicted and measured splitting matrices for the coupled mode pair ${}_2S_0/{}_7S_2$ are shown in Fig. 11. Note the large element in the real part of the off-diagonal cross-coupling block that is

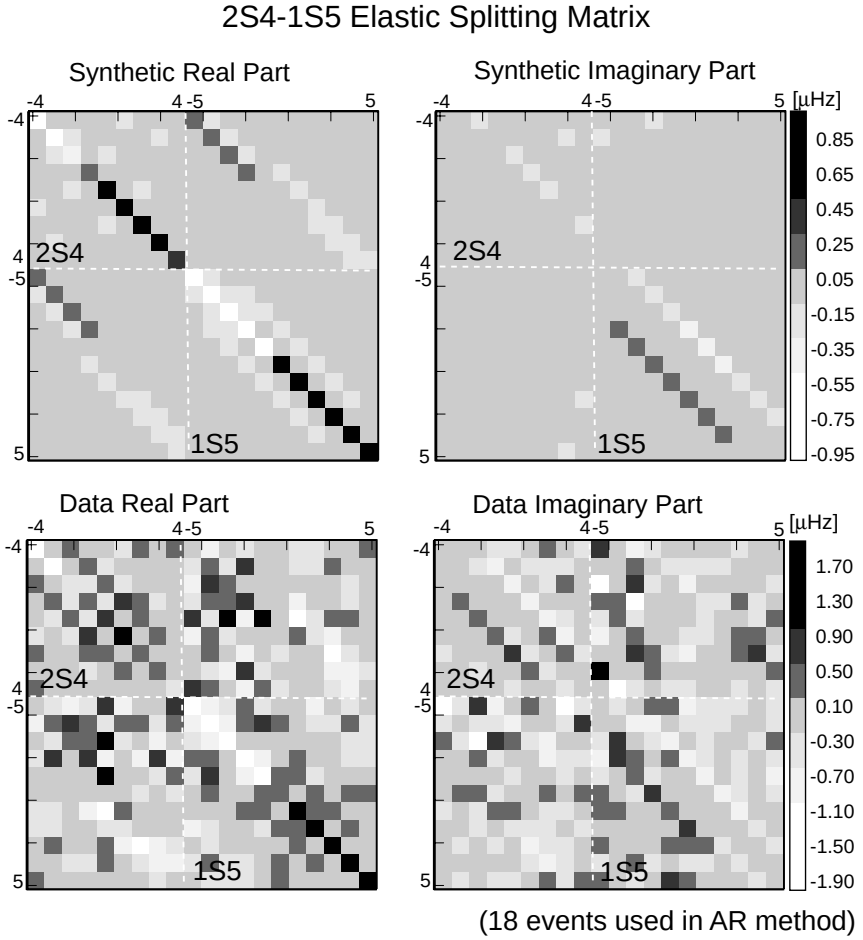

Figure 9. Predicted and measured elastic splitting matrix **E** of the coupled mode pair ${}_1S_5/{}_2S_4$. Note that the signal in the diagonal self-coupling blocks is generally somewhat larger in the observations than in the predictions. Also note that some predicted features show up in the measured off-diagonal cross-coupling blocks (e.g. dark at upper left corner, light towards the lower right) but that the SNR is probably still too low to extract reliably odd harmonic structure from these blocks.

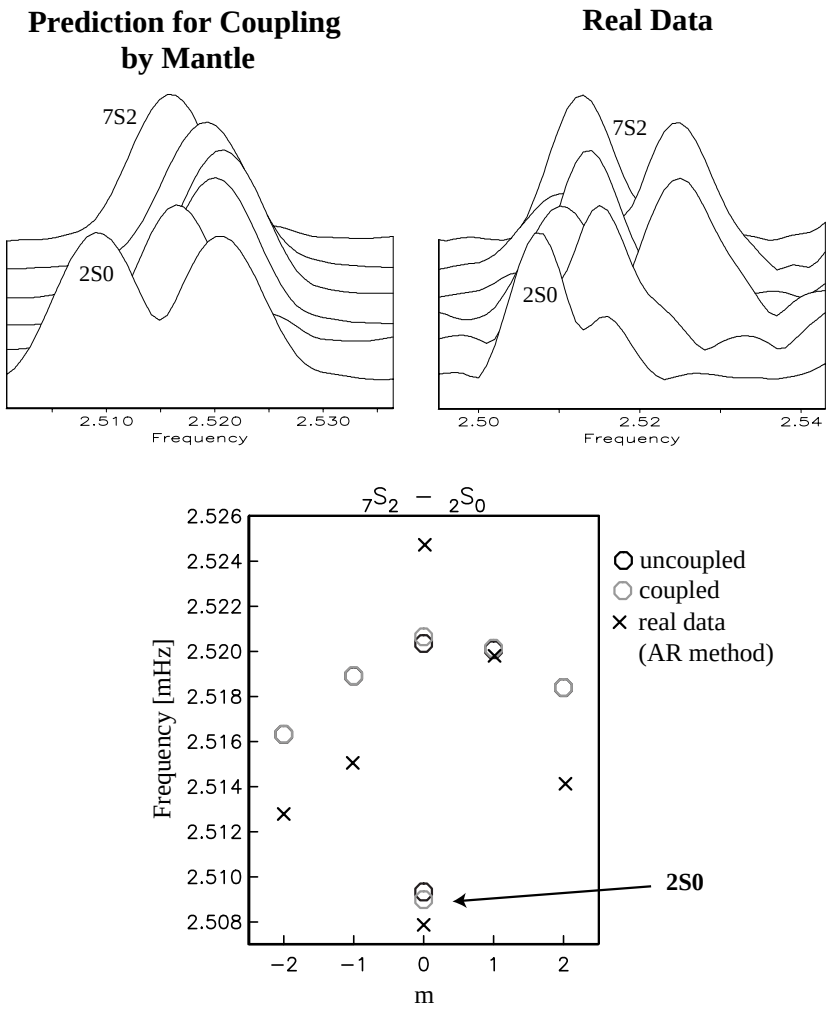

Figure 10. (Top) Synthetic (left) and measured (right) receiver strips for the strongly coupled mode pair ${}_2S_0/{}_7S_2$ for the 1994 Bolivia event. The synthetic strips were calculated considering rotation and hydrostatic ellipticity of the Earth as well as aspherical mantle structure (S16B30; Masters *et al.* 1996). The procedure no longer visually separates the two modes and some of the $m=0$ line of ${}_7S_2$ appears to be mapped into the strip of ${}_2S_0$. (Bottom) Theoretical and measured singlet frequencies for mode pair ${}_2S_0/{}_7S_2$. Coupling causes the frequencies of ${}_2S_0$ and the $m=1$ line of ${}_7S_2$ to repel each other. The singlet frequencies measured with the AR method are also given. Note that mode ${}_7S_2$ is anomalously split (presumably due to inner core structure).

common to both predicted and measured matrices. This row and column contain information for $s=2$.

CONCLUSIONS

The study of the splitting and coupling of free oscillations can potentially provide some unique information about the Earth. The rapid expansion of the global seismic network and the occurrence of many large (and deep) earthquakes in the past few years means that mode splitting analyses are capable of much higher precision than in the past. We believe that the precision needed to discuss the 3-D density structure of the Earth and its 3-D anelastic structure is within our reach. We propose a new technique (the matrix AR method) to perform this analysis. We have demonstrated that the method works and it has the significant advantage that it requires no information about the source. This means that we can analyse higher-frequency modes than have been attempted in the past, and that we avoid the trade-off between source size and attenuation that can afflict other techniques.

ACKNOWLEDGMENTS

This research was made possible by the dedicated work of the personnel who run global seismic networks: Geoscope, IDA, IRIS, Mednet, Geofon, BFO and the USGS, and by the IRIS and Geoscope data centers, which greatly facilitate access to the data. We gratefully acknowledge support by grants EAR96-28494, EAR95-08113 and EAR97-06056 from the National Science Foundation. The compilation of structure coefficients used in this paper can be obtained from the authors (gmasters@ucsd.edu).

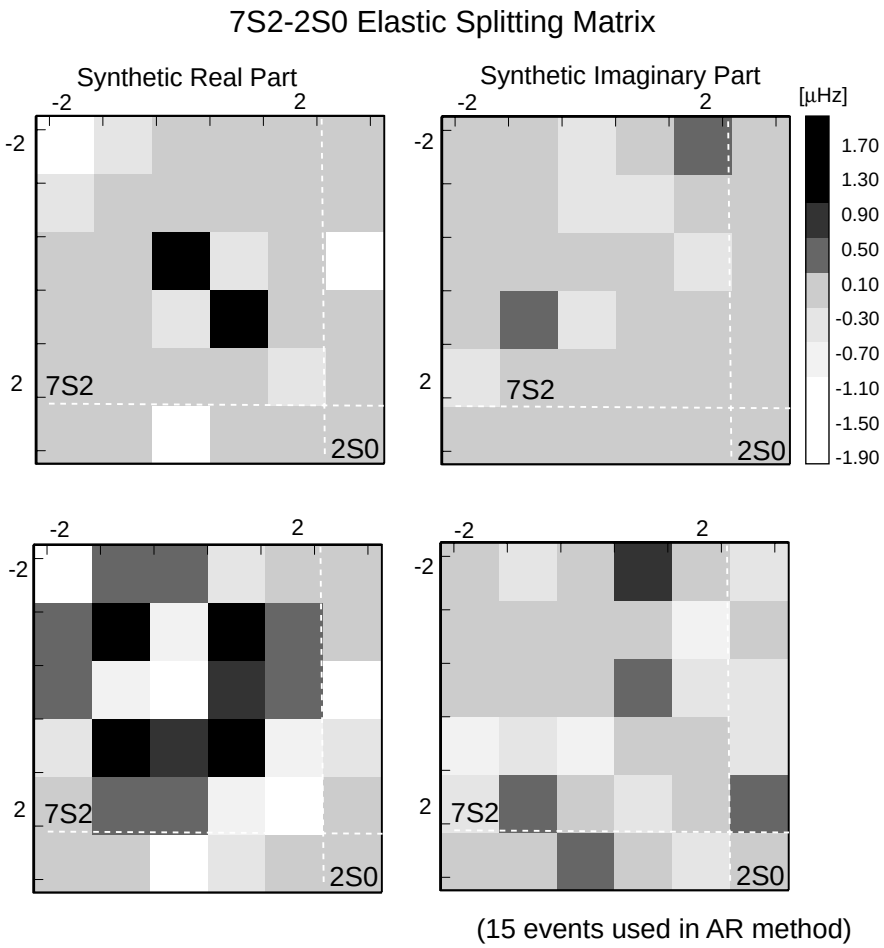

Figure 11. Predicted and measured splitting matrix of the coupled mode pair ${}_2S_0/{}_7S_2$. Note the large element in the real part of the off-diagonal cross-coupling block that is common to both predicted and measured matrices. The signal in the ${}_7S_2$ self-coupling blocks is much larger in the observations than in the predictions due to effects of inner core structure. Note that the traces in the diagonal self-coupling block are individually made zero, hence the (6, 6) element of **E** does *not* represent the frequency of ${}_2S_0$.

REFERENCES

Dahlen, F.A. & Tromp, J., 1998. *Theoretical Global Seismology,* Princeton University Press, Princeton, NJ.

Giardini, D., Li, X.-D. & Woodhouse, J.H., 1987. Three-dimensional structure of the earth from splitting in free oscillation spectra, *Nature,* **325,** 405–411.

Giardini, D., Li, X.-D. & Woodhouse, J.H., 1988. Splitting functions of long period normal modes of the earth, *J. geophys. Res.,* **93,** 13 716–13 742.

Gilbert, F. & Woodhouse, J.H., 2000. Determination of structure coefficients from splitting matrices, *Geophys. J. Int.,* **142,** 1–3.

He, X. & Tromp, J., 1996. Normal mode constraints on the structure of the Earth, *J. geophys. Res.,* **101,** 20 053–20 082.

Henson, I.H., 1989. Multiplet coupling of the normal modes of an elliptical, transversely isotropic Earth, *Geophys. J. Int.,* **98,** 457–459.

Ishii, M. & Tromp, J., 1999. Normal mode and free-air gravity constraints on lateral variations in velocity and density of Earth's mantle, *Science,* **285,** 1231–1236.

Kellogg, L.H., Hager, B.H. & van der Hilst, R.D., 1999. Compositional stratification in the deep mantle, *Science,* **283,** 1881–1884.

Landau, L.D. & Lifshitz, E.M., 1958. *Quantum Mechanics,* Addison Wesley, Reading, MA.

Laske, G. & Masters, G., 1999. Limits on differential rotation of the inner core from an analysis of the Earth's free oscillations, *Nature,* **402,** 66–69.

Masters, G., Johnson, S., Laske, G. & Bolton, H., 1996. A shear velocity model of the mantle, *Phil. Trans. R. Soc. Lond.,* **A354,** 1385–1411.

Masters, G., Laske, G. & Gilbert, F., 2000a. Autoregressive estimation of the splitting matrix of free-oscillation multiplets, *Geophys. J. Int.,* **141,** 25–42.

Masters, G., Laske, G., Bolton, H. & Dziewonski, A., 2000b. The relative behavior of shear velocity, bulk sound speed, and compressional velocity in the mantle: implications for chemical and thermal structure, *Seismology and Mineral Physics, AGU Monogr.,* Vol. 117, pp. 63–87, eds Karato, S.-I., Forte, A., Liebermann, R., Masters, G. & Stixrude, L., Washington, DC, in press.

Park, J., 1990. Radial mode observations from the 5/23/89 Macquarie Ridge earthquake, *Geophys. Res. Lett.,* **17,** 1005–1008.

Park, J. & Gilbert, F., 1986. Coupled free oscillations of an aspherical dissipative rotating earth: Galerkin theory, *J. geophys. Res.,* **91,** 7241–7260.

Resovsky, J.S. & Ritzwoller, M.H., 1998. New and refined constraints on three-dimensional Earth structure from normal modes below 3 mHz, *J. geophys. Res,* **103,** 783–810.

Ritzwoller, M., Masters, G. & Gilbert, F., 1986. Observations of anomalous splitting and their interpretation in terms of aspherical structure, *J. geophys. Res.,* **91,** 10 203–10 228.

Ritzwoller, M., Masters, G. & Gilbert, F., 1988. Constraining aspherical structure with low frequency interaction coefficients: application to uncoupled multiplets, *J. geophys. Res.,* **93,** 6369–6396.

Smith, M.F. & Masters, G., 1989. Aspherical structure constraints from free oscillation frequency and attenuation measurements, *J. geophys. Res.,* **94,** 1953–1976.

Su, W.-J. & Dziewonski, A.M., 1997. Simultaneous inversion for 3D variations in shear and bulk velocity in the mantle, *Phys. Earth planet. Inter.,* **100,** 135–156.

Woodhouse, J.H., 1980. The coupling and attenuation of nearly resonant multiplets in the earth's free oscillation spectrum, *Geophys. J. R. astr. Soc.,* **61,** 261–283.

Woodhouse, J.H. & Dahlen, F.A., 1978. The effect of a general aspherical perturbation on the free oscillations of the earth, *Geophys. J. R. astr. Soc.,* **53,** 335–354.

Woodhouse, J.H. & Girnius, T.P., 1982. Surface waves and free oscillations in a regionalized earth model, *Geophys. J. R. astr. Soc.,* **68,** 653–673.

Woodhouse, J.H., Giardini, D. & Li, X.-D., 1986. Evidence for inner core anisotropy from splitting of free oscillation data, *Geophys. Res. Lett.,* **13,** 1549–1552.

APPENDIX A: CORIOLIS COUPLING AND SPLITTING PARAMETERS

We shall make reference to Appendix D of Dahlen & Tromp (1998). We write U, V for the displacement scalers u, v in their notation. Let us write the elastic splitting matrix in the form

$$\mathbf{E} = \mathbf{E}^{3D} + \mathbf{W} + (\mathbf{V}^{ell+cen} - \omega_0^2 \mathbf{T}^{ell})/2\omega_0 \,, \tag{A1}$$

where ω_0 (sometimes written $\bar{\omega}$) is the reference or fiducial frequency for a set of coupled multiplets. The effects of $\mathbf{V}^{ell+cen} - \omega_0^2 \mathbf{T}^{ell}$ cannot be distinguished from those of aspherical structure (c_2^0) and it is customary to calculate $\mathbf{V}^{ell+cen} - \omega_0^2 \mathbf{T}^{ell}$ for a 1-D model and subtract it from eq. (A1) so that

$$\mathbf{E} = \mathbf{E}^{3D} + \mathbf{W} \,. \tag{A2}$$

In eq. (A2), $\mathbf{E}^{3D}$ is the elastic splitting matrix due to 3-D structure and $\mathbf{W}$ is due to the Coriolis force.

For a split spheroidal multiplet (a self-coupled block of $\mathbf{E}$), the diagonal of $\mathbf{E}^{3D}$ is symmetric in m because it represents axisymmetric structure. It is well known that $\mathbf{W}$ in this case is diagonal and linear in m. Let

$$\phi_m = 3m/[(2\ell+1)\ell(\ell+1)] \,. \tag{A3}$$

Then

$$\sum_m \phi_m E^{3D}_{mm} = 0 \tag{A4}$$

and

$$\sum_m \phi_m W_{mm} = \sum_m E_{mm} = \chi\Omega \,, \tag{A5}$$

where χ is the Coriolis splitting parameter,

$$\chi = \int_0^a \rho(r)[V^2 + 2UV]r^2 \, dr \,. \tag{A6}$$

We see that χ can be determined from the splitting matrix. It is a linear integral constraint on the 1-D density.

For a Coriolis-coupled spheroidal–toroidal pair of multiplets ${}_nS_l$ and ${}_{n'}T_{l'}$ we must have $\ell' = \ell \pm 1$. In this case the diagonal of the coupling block of $\mathbf{E}$ for which $t = 0$ ($m' = m$) is odd in m. Let

$$\phi_m = 3(\delta_{\ell\ell'+1} S_{\ell m}/\ell + \delta_{\ell\ell'-1} S_{\ell' m}/\ell') \,, \tag{A7}$$

where $S_{\ell m} = [(\ell+m)(\ell-m)/(2\ell+1)(2\ell-1)]^{1/2}$. Then, eq. (A4) is again true and

$$\sum_m \phi_m E_{mm} = -i\zeta\Omega \,, \tag{A8}$$

where ζ is the Coriolis coupling parameter,

$$\zeta = \int_0^a \rho(r) W^A(r) r^2 \, dr \,, \tag{A9}$$

and $W^A(r)$ is given in eq. (D.71) of Dahlen & Tromp (1998). We see that ζ, like χ, is a linear constraint on the 1-D density. Both can be recovered from $\mathbf{E}$.

Every spheroidal multiplet ($\ell > 0$) is a potential source for a value of χ and every Coriolis-coupled spheroidal–toroidal pair is a potential source for a value of ζ. There are hundreds of the former and many tens of the latter below 5 mHz. Consequently, it is reasonable to expect to be able to resolve the 1-D density with great accuracy in the not too distant future. It is equally reasonable to expect to be able to estimate the moment of inertia of the 1-D earth model.